Supporting Information

Electro-chemo-mechanical effect in Gd-doped Ceria thin films with a controlled orientation

Simone Santucci[a)], *Haiwu Zhang*[a)], *Simone Sanna*[b)], *Nini Pryds*[a)], *Vincenzo Esposito**[a)]

S. Santucci, Dr. H. Zhang, Dr. S. Sanna, Prof. N. Pryds, Prof. V. Esposito

a) Department of Energy Conversion and Storage, Technical University of Denmark, Fysikvej, Building 310, 2800 Kgs. Lyngby, Denmark.

b) Dipartimento di Ingegneria Civile e Ingegneria Informatica and CNR-SPIN, Università di Roma Tor Vergata, Via del Politecnico 1, I-00133 Roma, Italy

E-mail: sisan@dtu.dk, vies@dtu.dk

Cantilever and calculation (M_{11} and M_{12}):

The electro-mechanical characterization is carried out by the cantilever vibration method with planar electrodes. **Fig. S1** shows the schematics of the beam geometry with a long size of X= 5 mm and width Y= 2.5 mm. The overall thickness is 100 µm. One side of the beam is glued to a base, while the other end is free to move. Two gold electrodes are placed at the top surface and have a size of ≈ 1 x 1 mm^2.

When an electric field is applied to the electrodes, the cantilever vibrates as a result of the electrostriction properties of the CGO films. In particular, the planar electrodes configuration allows to trigger the in-plane electrostriction effect along both longitudinal (*i.e.* M_{11}) and transverse (M_{12}) electrostriction directions. Nigon et al. showed that for planar electrode configuration the effective electric field is reduced in the film: $E= V/[(x_0 - x_1)+\Delta a]$, where $(x_0 - x_1)$ is the gap between electrodes

(500 μm) and Δa is a factor that depends on the film thickness: $\Delta a = 1.324 \cdot t_f$ [1]. Since in our case Δa << (x_0 - x_1), we can neglect this correction. Moreover, we consider the area of the film under the electrodes to be passive as there the electric field is strongly reduced [1,2]. Nguyen et al. examined the substrate contribution in planar electrodes configuration [2]. They showed that the electric field is high only in the film, and the wafer effect is noticeable only if a bottom electrode is introduced. The applied electric field is considered constant along the vertical direction as the thickness of the sample is low compared to the in-plane size of the sample. This formalism is widely accepted, and the approximation is supported by in planar impedance spectroscopy experiments [3–6].

Fig. S1 shows the geometrical factor of the cantilever and the gap between the two electrodes (500 μm), reported as x_0 - x_1. x_0 is defined as 0 by experimental design. As the only electroactive part of the film is the gap, the vertical oscillation *d* is measured at x_1. In order to calculate the longitudinal electrostriction coefficient (M_{11}), the displacement is measured in a fixed position with different electric fields (*d vs E*). Then, the curvature Δk is calculated from:

$$d(x_1) = \frac{x_1^2}{2 \cdot \Delta k} \#S1$$

For the shear electrostriction coefficient M_{12}, the vertical displacement is measured along the sample width (Y-scan). A second-order polynomial fit is used to obtain the trend. The curvature of the parabolic profile of the displacement is then calculated with the equation:

$$\Delta k = \frac{2a}{\left(1 + (2ay + b)^2\right)^{3/2}} \#S2$$

Considering $d = ay^2+by+c$, with z vertical displacement and y width position. The lowest curvature radius in the parabola is considered.

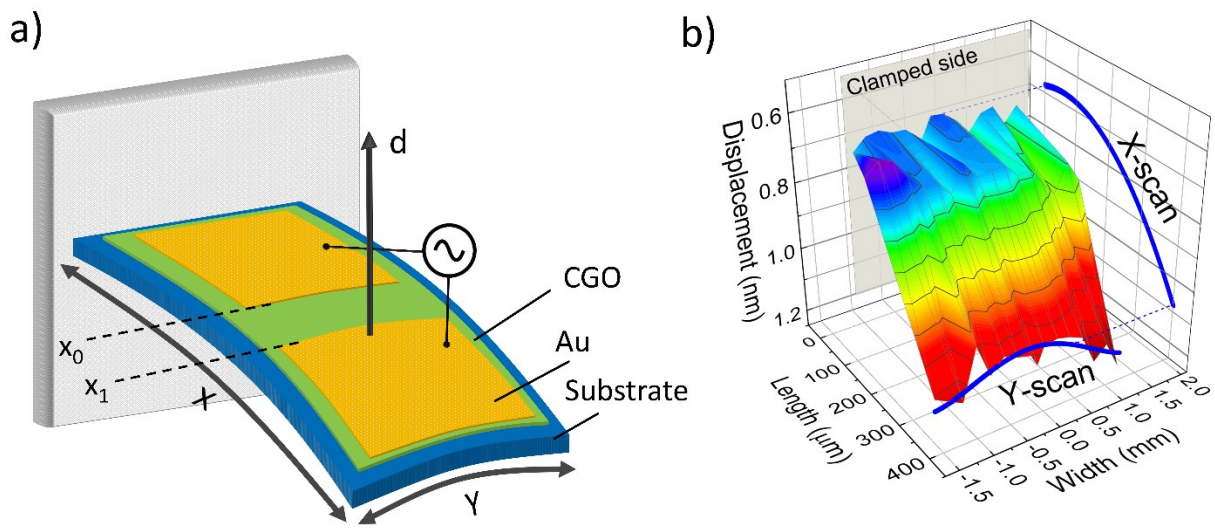

Fig. S1. Cantilever beam geometry and operation. *a)* Schematic of the samples. The vertical displacement *d* is measured while applying a voltage to the planar gold electrodes. M_{11} is calculated measuring *d* while increasing the electric field, M_{12} is calculated by shear scans along the width of the sample (Y-scan). *b)* Deformation map of CGO film, for 16 kV/cm applied field with 1 Hz frequency. The distortion takes place both along the length (X-scan) and the width (Y-scan).

The in-plane stress is evaluated with the Stoney formula [7–10].

$$\Delta\sigma = \frac{Y_s \quad t_s^2}{1 - v_s 6 t_f} \Delta k \# S3$$

Where Y_s and ν_s are Young's modulus and the Poisson ratio of the substrate and t_s and t_f are the thickness of the substrate and film, respectively. We considered Y= 230 GPa and ν= 0.31 for YSZ [11–13], Y= 270 GPa and ν= 0.33 for STO [14–17] and Y= 200 GPa and ν= 0.29 for NGO [17,18]. The

Stoney formula is used to calculate in-plane stress in films deposited on a thick substrate so it does not differ in planar electrode configuration.

The value of M is obtained using a linear fit of stress versus the squared field, following the equation:

$$M = \frac{\Delta\sigma}{E^2 \cdot Y} \#S4$$

Where Y is Young´s modulus of CGO, assumed the bulk elastic constant Y= 200 GPa as reported in literature also in the case of thin films [8,10,12,19,20].

In order to exclude the thermal contribution to the oscillation, an Optris PI thermal camera with a sensitivity of 0.1 mK is used to detect potential temperature differences. However, no heating is observed. We use the current monitor of the Trek voltage amplifier during the application of the electric field. The current is always below the resolution of the instrument (< 3μA). High electric fields can cause other effects such as polarization or electrostatic force (*i.e.* Maxwell stress tensor), so the bare substrates were also characterized by the same method, followed by subtraction of their contributions (Fig. S7-8-9).

Lock-in amplifier measurements:

In our setup, the lock-in amplifier is connected to a USB data acquisition (DAQ) device. A Labview program has been made to control and manage the data. Then, the signal is converted from mV to nm by the instrument's conversion factor reported in the datasheet provided by the manufacturer. As a result, the precision of the measurements was improved significantly. However, accuracy is frequency-dependent. For signals with f <3 Hz or f > 100 Hz, the achieved resolution goes down to 0.2 nm,

allowing the detection of rather small oscillations. To detect electrostriction oscillation, we chose frequency to be twice the frequency of the applied field. **Fig. S2** shows the measurement performed on a CGO/YSZ sample for voltages from 0 to 3 V. The magnitude of the oscillation at the selected frequency is measured continuously and displayed as a function of time. The sampling frequency is usually between 100 to 1000 Hz, and the measurement time is 5 minutes. The values measured (100 values/sec for 5 minutes) are averaged to obtain an accurate evaluation of oscillation. The raw amplifier output is in mV, and it is converted to displacement by conversion factors characteristic of the instrument model. The implementation of a lock-in amplifier brings several improvements to the setup besides increasing the resolution. The external drift is cancelled from the analysis automatically because it is a static effect. However, this process is sensible to only one frequency per measurement. Therefore, one-time events, static contribution, or double harmonic oscillations are not detectable with this technique.

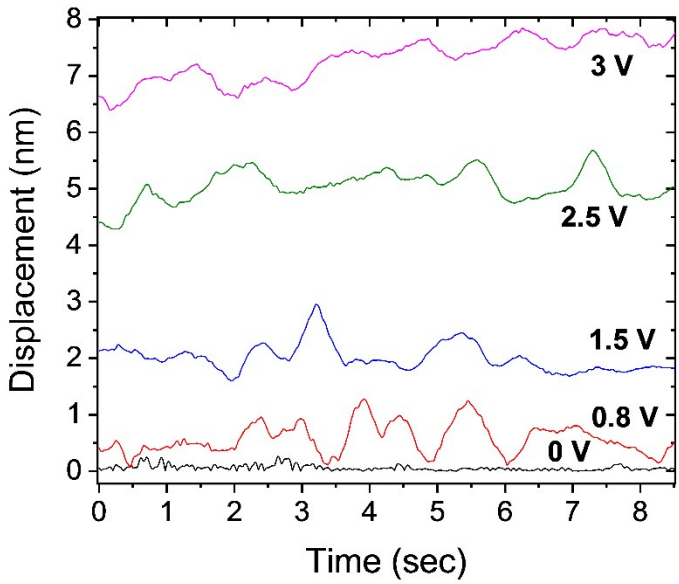

Fig. S2: Measurement of 1 Hz oscillation amplitude of CGO/YSZ with increasing voltages (at 0.5 Hz) performed with the lock-in amplifier. The displacement values refer to the contribution of 1 Hz oscillation. The frequency chosen is double the electric field frequency because electrostriction vibration depends on the second harmonic.

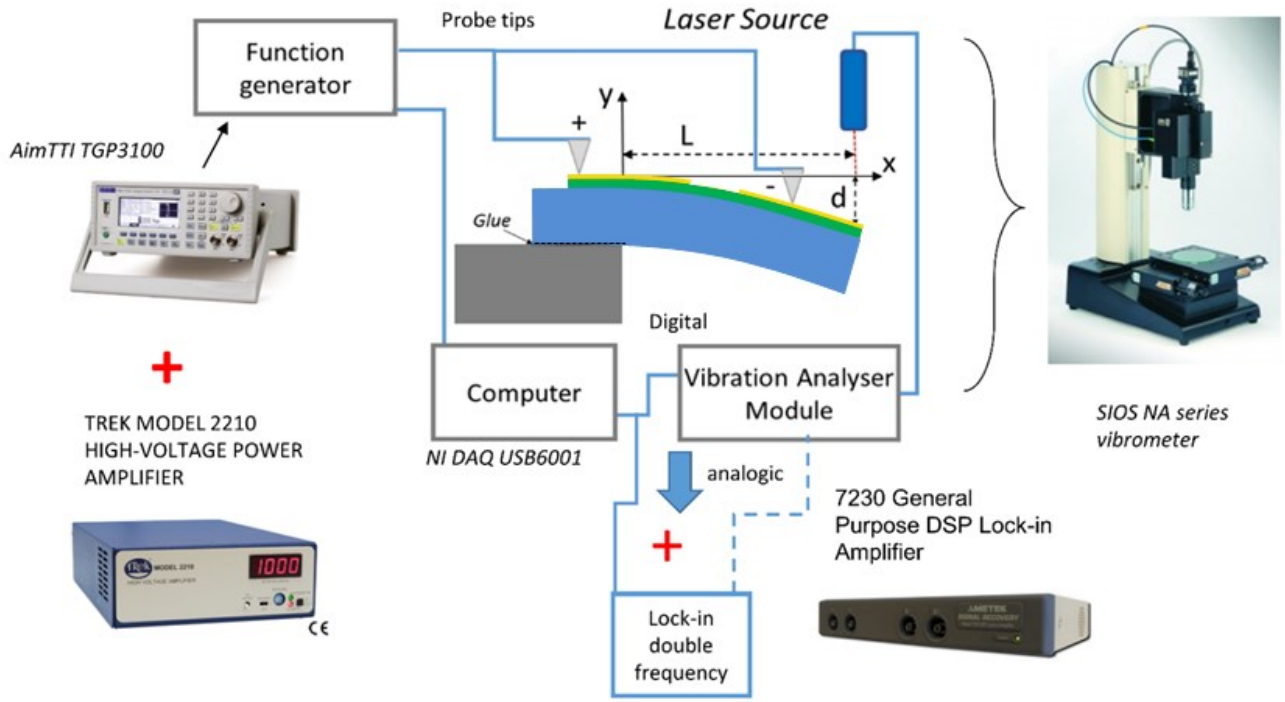

Fig. S3: Schematic of the setup with this work new add-ons. The sample sketch includes the substrate (blue), film (green) and electrodes (yellow).

Substrate-film geometry and electrodes configuration:

To apply electric field along a chosen in-plane direction, we need to place the electrodes on the surface, parallel to it. By changing the geometry of the top electrodes, we can choose in which direction to apply the electric field, without growing samples with different orientation. **Fig. S4** shows the geometry of a CeO_2 cell on top (100) plane of an NGO substrate (grey). The (100) plane of the pseudocubic NGO cell match (dotted line) with CGO cell along (111) direction, resulting in (111) vertical orientation and in-plane [0-11] and [-211] orthogonal directions. Therefore, we applied the surface electrodes in two configurations: one along [0-11] direction (black dashed arrow in figure S4) and one along [-211] (red dashed arrow). **Fig. S5** shows the geometry of a CeO_2 cell on top (100) plane

of an STO substrate (grey). For $CGO_{100}/STO_{100,}$ only one configuration along the [011] direction was used. **Fig. S6** shows the geometry of a CeO_2 cell on top (110) plane of a YSZ substrate (grey). In this sample, we used one configuration along the [001] crystal direction (black dashed arrow) and one diagonal along the [-223] direction (red dashed arrow) by placing the electrodes with an angle of ≈45°.

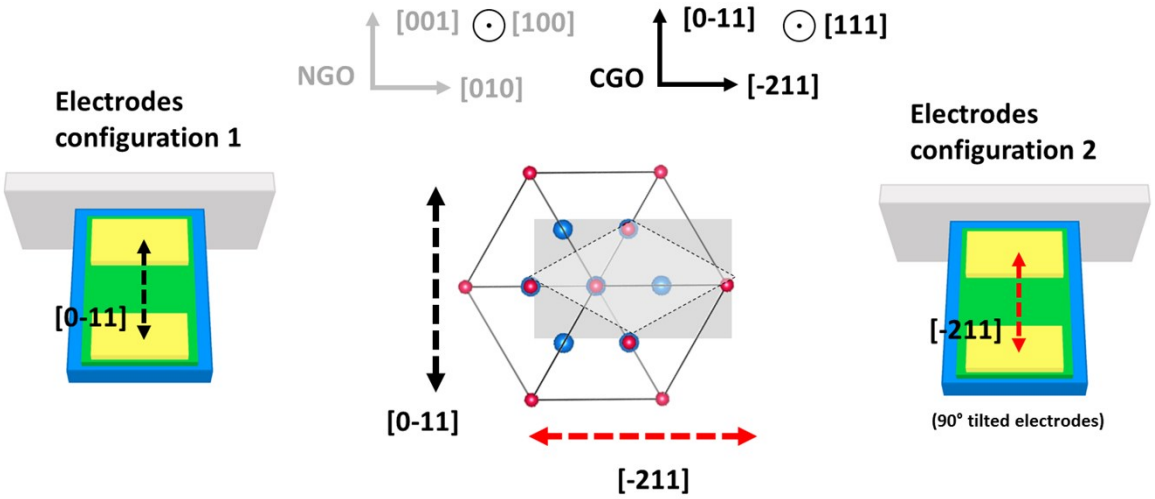

Fig. S4: Top view of CeO_2 cell on NGO (100) plane (grey). The NGO pseudocubic cell is highlighted by the dashed rectangle. The grey and black arrows report the orientation of NGO and CGO, respectively. *Electrodes configuration 1*: configuration of the electrodes to excite the crystal along [0-11] direction, depicted by the black dashed line. *Electrodes configuration 2*: configuration of the electrodes for [-211] direction, represented by the red dashed line.

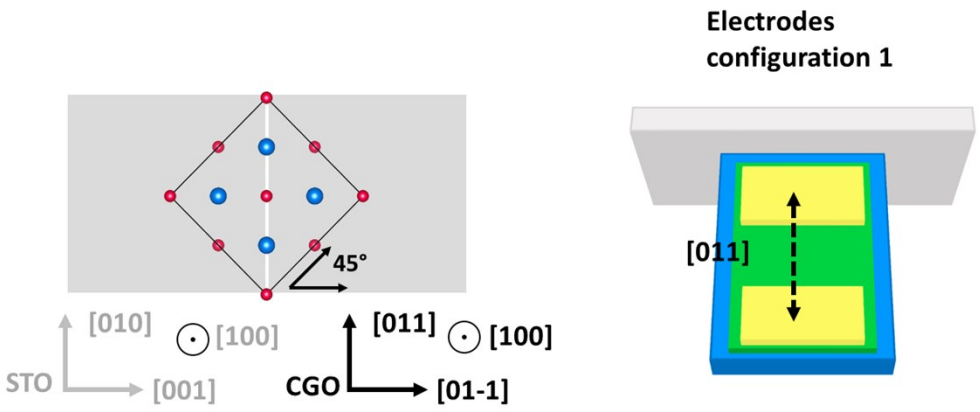

Fig. S5: Top view of CeO_2 cell on STO(100) plane (grey). The grey and black arrows report the orientation of STO and CGO, respectively. CGO film grows 45° tilted respect to the substrate.

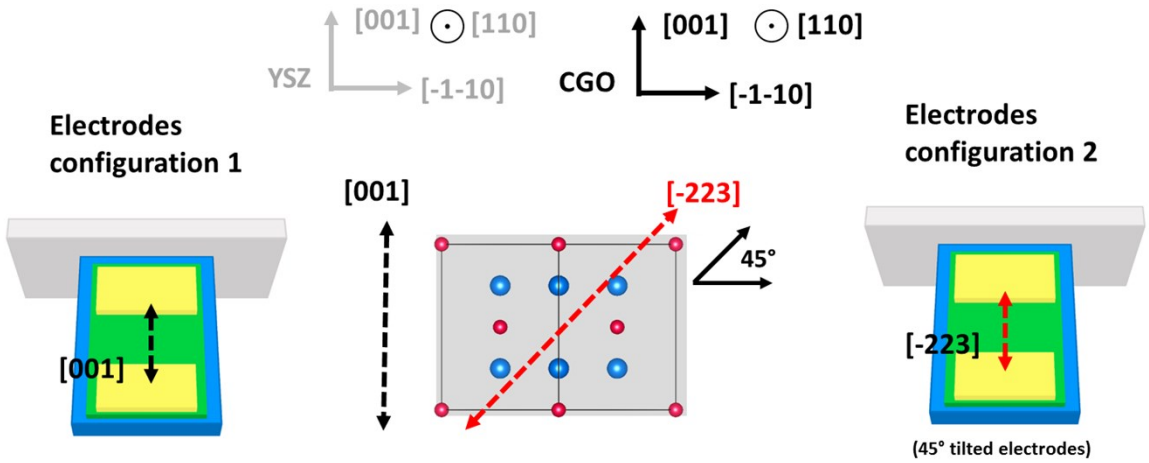

Fig. S6: Top view of CeO_2 cell on YSZ (110) plane (gray). The grey and black arrows report the orientation of YSZ and CGO, respectively. *Electrodes configuration 1*: configuration of the electrodes to excite the crystal along [001] direction, depicted by the black dashed line. *Electrodes configuration 2*: configuration of the electrodes for [-223] direction, represented by the red dashed line.

Substrate characterization:

In order to exclude side effects of YSZ STO and NGO, the substrates were characterized alone, with Au gold electrodes and the method described in the paper. The values of stress, displacement and electrostriction coefficient reported in the article are all reported after subtracted the substrate contribution. The values indicating the substrate contributions were obtained by fitting the displacement vs E squared and calculating the slope of the line. This value was subtracted to the slope of the strain in samples with films; then it was converted in stress vs E squared, that is the electrostriction coefficient. No current was detected above the DAQ 6001 resolution ≈ 3 μA.

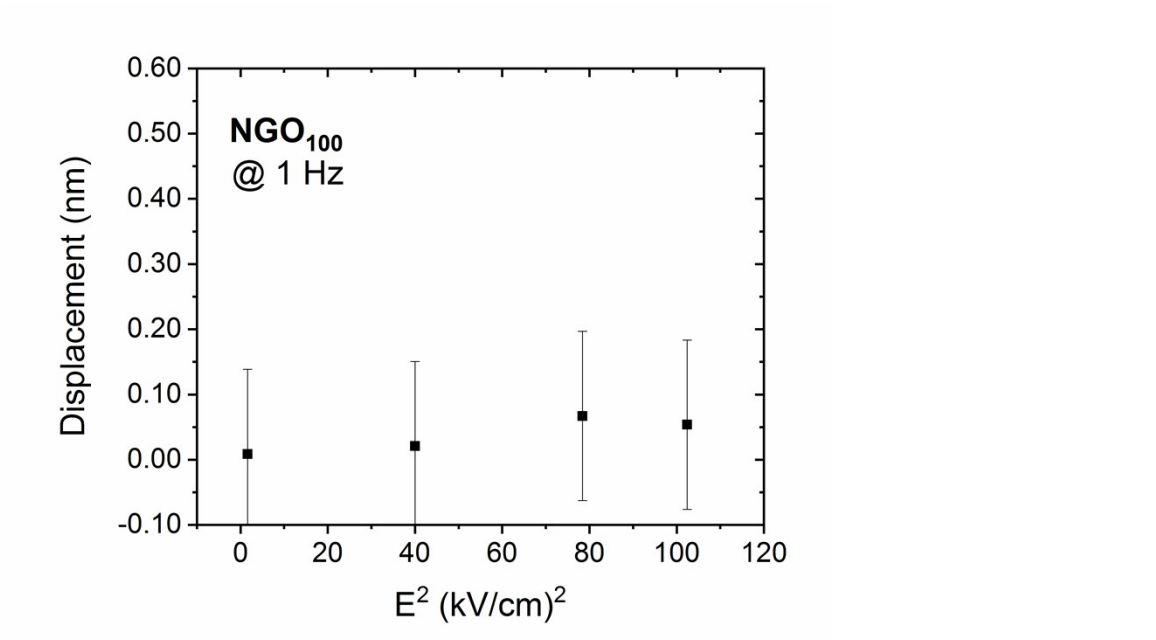

Fig. S7: Displacement of $NGO_{(100)}$ substrate for 1 Hz electric field. No contribute was considered as NGO did not show any response to the electric field.

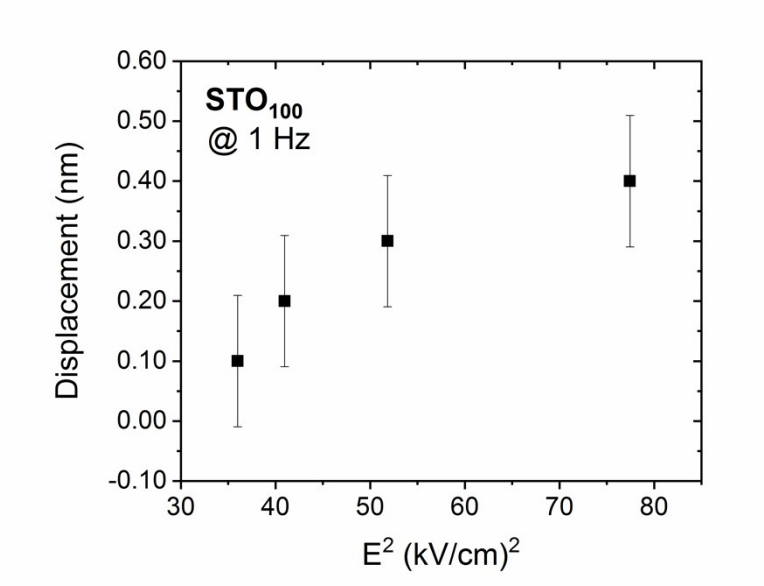

Fig. S8: Displacement of $STO_{(100)}$ substrate for 1 Hz electric field. It contributes to the $CGO_{(100)}/STO_{(100)}$ oscillation by 10%.

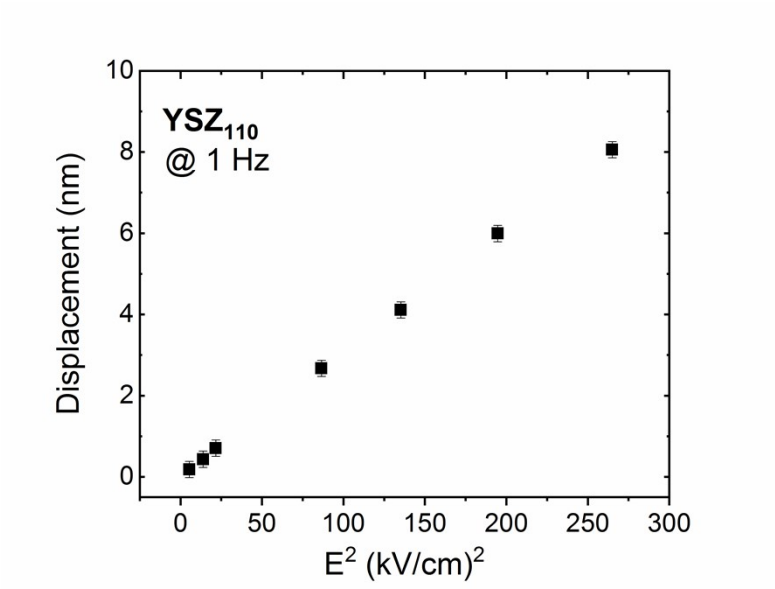

Fig. S9: Displacement of YSZ(110) substrates for 1 Hz electric field. The displacement of YSZ alone represents about 50% of the total displacement of the CGO(110)/YSZ(110) sample.

References:

[1] R. Nigon, T.M. Raeder, P. Muralt, Characterization methodology for lead zirconate titanate thin

films with interdigitated electrode structures, J. Appl. Phys. 121 (2017). https://doi.org/10.1063/1.4983772.

[2] C.H. Nguyen, R. Nigon, T.M. Raeder, U. Hanke, E. Halvorsen, P. Muralt, Probing-models for interdigitated electrode systems with ferroelectric thin films, J. Phys. D. Appl. Phys. 51 (2018). https://doi.org/10.1088/1361-6463/aab2a1.

[3] K. Rodrigo, S. Heiroth, M. Lundberg, N. Bonanos, K. Mohan Kant, N. Pryds, L. Theil Kuhn, V. Esposito, S. Linderoth, J. Schou, T. Lippert, Electrical characterization of gadolinia-doped ceria films grown by pulsed laser deposition, Appl. Phys. A Mater. Sci. Process. 101 (2010) 601–607. https://doi.org/10.1007/s00339-010-5975-7.

[4] A. Bieberle-Hütter, J.L. Hertz, H.L. Tuller, Fabrication and electrochemical characterization of planar Pt-CGO microstructures, Acta Mater. 56 (2008) 177–187. https://doi.org/10.1016/j.actamat.2007.09.006.

[5] I. Kosacki, T. Suzuki, V. Petrovsky, H.U. Anderson, Electrical conductivity of nanocrystalline ceria and zirconia thin films, Solid State Ionics. 136–137 (2000) 1225–1233. https://doi.org/10.1016/S0167-2738(00)00591-9.

[6] S. Sanna, V. Esposito, D. Pergolesi, A. Orsini, A. Tebano, S. Licoccia, G. Balestrino, E. Traversa, Fabrication and electrochemical properties of epitaxial samarium-doped ceria films on SrTiO3-buffered MgO substrates, Adv. Funct. Mater. 19 (2009) 1713–1719. https://doi.org/10.1002/adfm.200801768.

[7] M.R. Ardigo, M. Ahmed, A. Besnard, Stoney Formula: Investigation of Curvature Measurements by Optical Profilometer, Adv. Mater. Res. 996 (2014) 361–366. https://doi.org/10.4028/www.scientific.net/AMR.996.361.

[8] S. Santucci, H. Zhang, S. Sanna, N. Pryds, V. Esposito, Enhanced electro-mechanical coupling of TiN/Ce 0.8 Gd 0.2 O 1.9 thin film electrostrictor, APL Mater. 7 (2019) 071104. https://doi.org/10.1063/1.5091735.

[9] R. Korobko, E. Wachtel, I. Lubomirsky, Cantilever resonator based on the electrostriction effect in Gd-doped ceria, Sensors Actuators, A Phys. 201 (2013) 73–78. https://doi.org/10.1016/j.sna.2013.06.021.

[10] R. Korobko, A. Patlolla, A. Kossoy, E. Wachtel, H.L. Tuller, A.I. Frenkel, I. Lubomirsky, Giant electrostriction in Gd-doped ceria, Adv. Mater. 24 (2012) 5857–5861. https://doi.org/10.1002/adma.201202270.

[11] G.P. Cousland, X.Y. Cui, A.E. Smith, A.P.J. Stampfl, C.M. Stampfl, Mechanical properties of zirconia, doped and undoped yttria-stabilized cubic zirconia from first-principles, J. Phys. Chem. Solids. 122 (2018) 51–71. https://doi.org/10.1016/j.jpcs.2018.06.003.

[12] A. Selçuk, A. Atkinson, Elastic properties of ceramic oxides used in solid oxide fuel cells (SOFC), J. Eur. Ceram. Soc. 17 (1996) 1523–1532. https://doi.org/10.1016/s0955-2219(96)00247-6.

[13] L. Kurpaska, M. Frelek-Kozak, K. Nowakowska-Langier, M. Lesniak, J. Jasinski, J. Jagielski,

Structural and mechanical properties of Ar-ion irradiated YSZ single-crystals grown in different crystallographic orientations, Nucl. Instruments Methods Phys. Res. Sect. B Beam Interact. with Mater. Atoms. 409 (2017) 81–85. https://doi.org/10.1016/j.nimb.2017.05.008.

[14] A.P. Sakhya, J. Maibam, S. Saha, S. Chanda, A. Dutta, B.I. Sharma, R.K. Thapa, T.P. Sinha, Electronic structure and elastic properties of ATiO3 (A = Ba, Sr, Ca) perovskites: A first principles study, Indian J. Pure Appl. Phys. 53 (2015) 102–109.

[15] O. Bernard, M. Andrieux, S. Poissonnet, A.M. Huntz, Mechanical behaviour of ferroelectric films on perovskite substrate, J. Eur. Ceram. Soc. 24 (2004) 763–773. https://doi.org/10.1016/S0955-2219(03)00324-8.

[16] K. Persson, Materials Data on SrTiO3 (SG:221) by Materials Project, (2014). https://doi.org/10.17188/1263154.

[17] M. De Jong, W. Chen, T. Angsten, A. Jain, R. Notestine, A. Gamst, M. Sluiter, C.K. Ande, S. Van Der Zwaag, J.J. Plata, C. Toher, S. Curtarolo, G. Ceder, K.A. Persson, M. Asta, Charting the complete elastic properties of inorganic crystalline compounds, Sci. Data. 2 (2015) 1–13. https://doi.org/10.1038/sdata.2015.9.

[18] K. Persson, Materials Data on NdGaO3 (SG:62) by Materials Project, (2014). https://doi.org/10.17188/1206007.

[19] R. Korobko, C.T. Chen, S. Kim, S.R. Cohen, E. Wachtel, N. Yavo, I. Lubomirsky, Influence of Gd content on the room temperature mechanical properties of Gd-doped ceria, Scr. Mater. 66 (2012) 155–158. https://doi.org/10.1016/j.scriptamat.2011.10.027.

[20] Y. Shi, S.C. Lee, M. Monti, C. Wang, Z.A. Feng, W.D. Nix, M.F. Toney, R. Sinclair, W.C. Chueh, Growth of Highly Strained CeO2 Ultrathin Films, ACS Nano. 10 (2016) 9938–9947. https://doi.org/10.1021/acsnano.6b04081.